# La2(Nb1-: XYx)2O7- δ: scovery of a novel fluorite structure-based ionic conductor

AUTHOR(S):

Han, Donglin; Kato, Kohei; Uda, Tetsuya

CITATION:

Han, Donglin ...[et al]. La2(Nb1-: XYx)2O7- δ: scovery of a novel fluorite structure-based ionic conductor. Chemical Communications 2017, 53(94): 12684-12687

ISSUE DATE:

2017-12-07

URL:

http://hdl.handle.net/2433/236386

To **Chemical Communications**

**Communication**

# $La_2(Nb_{1-x}Y_x)_2O_{7-\delta}$: Discovery of a Novel Fluorite Structure Based Ionic Conductor

Donglin Han [a, *], Kohei Kato [a], and Tetsuya Uda [a *]

[a] Department of Materials Science and Engineering, Kyoto University,

Yoshida Honmachi, Sakyo-ku, Kyoto 606-8501, Japan

* Corresponding author: Donglin Han (han.donglin.8n@kyoto-u.ac.jp)

Tetsuya Uda (uda_lab@aqua.mtl.kyoto-u.ac.jp)

TEL: +81-75-753-5445, FAX: +81-75-753-5284

**Abstract**

A novel fluorite structure-based compound of $La_2(Nb_{1-x}Y_x)_2O_{7-\delta}$ shows superior chemical stability, and proton conduction.

Benefitting from the ability of directly converting chemical energy from fuels (typically react with oxygen) into electricity, fuel cells possess several attractive advantages, including high energy conversion efficiency and low emission. Currently, proton exchange membrane fuel cells (PEMFCs) and solid oxide fuel cells (SOFCs) are the two representative types received commercialization, but promotion of their further application faces several obstacles mainly from the difficulty in cost reduction. For example, the PEMFCs use proton conductive polymer electrolyte weak in thermal tolerance [1], and typically operate at low temperature around 80 $^oC$. Such low operation temperature causes problem on fuel flexibility and catalyst activity, demanding high pure hydrogen fuel [1] and expensive platinum catalyst [2]. In contrary, SOFCs do not have such problem due to their high operation temperature (750 – 1000 $^oC$), which is needed to generate sufficient oxide ion conductivity in their ceramic-type electrolyte [3,4], but simultaneously, also introduces severe challenge on developing proper structural materials.

Working at intermediate temperature range (400 – 700 $^oC$), the fuel cells using proton-conductive ceramic-type electrolyte, which are commonly named as protonic ceramic fuel cells (PCFCs) [5], provide an alternative solution. Presently, yttrium-doped barium cerate ($Ba(Ce_{1-x}Y_x)O_{3-\delta}$,

BCY) and barium zirconate ($Ba(Zr_{1-x}Y_x)O_{3-\delta}$, BZY) receive the most attention, due to their high proton conductivity (> 0.01 $Scm^{-1}$ at 600 $^oC$ in moist atmosphere) [6-11]. However, the component of alkaline earth elements raises uncertainty on chemical stability. [12] BCY is known to be unstable against $CO_2$ or $H_2O$ [13-15]. BZY is generally regarded to be chemically stable, but recent work of Sažinas, *et al.* [16] revealed that in pure $CO_2$ atmosphere the BZY on surface changed to BaO-deficient perovskite with formation of $BaCO_3$, and this might affect the long-term stability.

As a strategy to further improve the chemical stability, significant effort has been dedicated on developing the electrolyte material free of the alkaline earth elements [12,17-26]. And special interest has been focused on oxides containing lanthanum and niobium [12,17,19]. As far as we know, there are two different composition systems exhibiting proton conduction. Shimura, *et al*, reported a fluorite-type oxide of Sr-doped $La_3NbO_{7-\delta}$, which is a mixed conductor of protons, oxide ions and electrons, showing the total conductivity around $1.2 \times 10^{-3}$ $Scm^{-1}$ in wet hydrogen at 700 $^oC$ [17]. And the oxide ion conduction predominates in the temperature range of 600 - 1000 $^oC$ [17]. Afterwards, Haugsrud and Norby discovered a fergusonite-type oxide system of acceptor-doped $LaNbO_4$ [12]. They found that the proton conduction was optimized by substituting 1 at% lanthanum with calcium. And the total conductivity is about $2.5 \times 10^{-4}$ and $4.3 \times 10^{-4}$ $Scm^{-1}$ at 600 and 700 $^oC$, respectively, in moist hydrogen. [16] In this work, we report a new oxide system with the composition of $La_2(Nb_{1-x}Y_x)_2O_{7-\delta}$, in which partial proton conduction was confirmed at the intermediate temperature range.

In addition to $La_2(Nb_{1-x}Y_x)_2O_{7-\delta}$, samples containing other elements including Sc, In, Nd, Sm, Gd and Yb were also tried for preparation, but only $La_2(Nb_{1-x}Y_x)_2O_{7-\delta}$ ($x$ = 0.6, 0.65, 0.7) was found to be of single phase after sintering at 1600 $^oC$ (see Table S1 and Fig. S1 in ESI). As shown in Fig. 1(a), a cubic disordered fluorite structure can be identified for $La_2(Nb_{0.3}Y_{0.7})_2O_{7-\delta}$, since its diffraction pattern matches well with that of a cubic fluorite oxide ($CeO_2$, JCPDS # 00-034-0394). However, in the XRD patterns of $La_2(Nb_{1-x}Y_x)_2O_{7-\delta}$ ($x$ = 0.6, 0.65), some small diffraction peaks ascribed to the feature of a cubic pyrochlore crystal structure appeared. The insects in Fig. 1(a) shows that peaks appearing at around14.1 and 35.9 $^o$ match the pyrochlore (331) diffraction peak ($La_2Zr_2O_7$, JCPDS # 01-070-5602). Since the pyrochlore structure is a fluorite-related structure with ordered arrangement of cations [27,28], such results imply that with the Y content increasing from 0.6 and 0.65 to 0.7, the cations possibly turn from an ordered arrangement to a disordered one. However, it is difficult to perform reliable structure analysis by refining the Cu $K\alpha$ diffraction patterns to determine some structural parameters, such as site occupancy of Y and Nb, since the scattering factors of Y and Nb are too close to be distinguished. Future work applying abnormal dispersion effect to collect XRD patterns is expected. Notation of $La_{0.5}Nb_{0.15}Y_{0.35}O_{2-\delta}$ might be more precise than the pyrochlore expression of $La_2(Nb_{0.3}Y_{0.7})_2O_{7-\delta}$, but for the sake of simplicity, we adopt $La_2(Nb_{0.3}Y_{0.7})_2O_{7-\delta}$ in this manuscript. EMPA-WDS was used to determine the composition of the as-sintered samples, which were found to agree with the nominal value (Table S2). And From Fig. 1(b), one can see that all these three samples exhibit sufficient grain growth after sintering.

Hydration reaction given in Eq. 1 is a basic route to introduce protons, which are charge carriers for the proton conduction, into oxide ceramics comprising diverse types of crystal structures. [7] Here, $V_O^{\bullet\bullet}$, $O_O^{\times}$ and $OH_O^{\bullet}$ are Kröger-Vink notation for oxide ion vacancies, lattice oxide ions and protons, respectively, indicating that oxide ion vacancies are essential for such hydration process. From the view point of defect chemistry, the concentration of oxide ion vacancies in $La_2(Nb_{1-x}Y_x)_2O_{7-\delta}$ can be calculated by assuming pentavalent Nb cations ( $Nb_{Nb}^{\times}$ ) being substituted by trivalent Y cations ( $Y_{Nb}^{''}$ ), as given in Eq. 2. Oxide ion vacancies thereby form to keep electroneutrality. The overall concentration of oxide vacancies is 1.2, 1.3, 1.4 per unit cell in the samples containing Y content of 0.6, 0.65, and 0.7, respectively. It has to be noted that there are two types of oxide ion vacancies in the pyrochlore-type oxides, namely, intrinsic and extrinsic oxide ion vacancies. [28] The concentration of extrinsic oxide ion vacancies (δ) in $La_2(Nb_{0.4}Y_{0.6})_2O_{7-\delta}$ and $La_2(Nb_{0.35}Y_{0.65})_2O_{7-\delta}$ is 0.2 and 0.3, respectively, while their intrinsic oxide ion vacancies have the same concentration of 1. The existence of oxide ion vacancies raises the possibility for hydration, which was also confirmed experimentally in this work. Fig. 2(a) shows the proton concentration measured after hydrating the samples in wet Ar ( $p_{H_2O} = 0.031$ atm ). One can see that the proton concentration changes little with the composition after hydration at 600 °C, and decreased slightly with the increasing Y content after hydration at 300 °C. However, roughly speaking, the proton concentration in all these three samples is around 0.07 and 0.04 after hydration at 300 and 600 °C, respectively. Furthermore, a clear phenomenon of chemical expansion due to the hydration [10,29-31] was observed; that is, as shown in Fig. 2(b), all these three

samples have relatively larger lattice constants in wet atmosphere, which is especially apparent at the temperature below 600 $^{o}$C. Since the dry Ar atmosphere used in this work is not absolutely free of water vapor, the samples get partially hydrated at lower temperature. The lattice constants thereby measured deviate from the dashed lines extrapolated from the data in high temperature range (700 – 1000 $^{o}$C). Following the extrapolated dashed lines, we were able to estimate the thermal expansion coefficient (TEC) in dry atmosphere, which is 1.07, 1.01, and 1.04 × $10^{-5}$ $K^{-1}$ for the samples with the Y content of 0.6, 0.65, and 0.7, respectively. We also compared the lattice constants of the as-sintered samples with those obtained by the HT-XRD measurements at 30 $^{o}$C (Fig. S2). One can see that the as-sintered samples have intermediate lattice constants, implying that the samples reported in this work are sensitive to water vapor, and possibly partially hydrated even in ambient atmosphere.

$$H_2O + V_O^{\bullet\bullet} + O_O^{\times} = 2OH_O^{\bullet} \quad (1)$$

$$2Nb_{Nb}^{\times} + Y_2O_3 + 2O_O^{\times} = Nb_2O_5 + 2Y_{Nb}^{''} + 2V_O^{\bullet\bullet} \quad (2)$$

Then, electrical impedance spectroscopy was applied to measure the conductivities of the samples, and all the spectra show only a single semicircle (an example is shown in Fig. S3), partially due to the large grain size and good combination of the grain boundary which makes the contribution of grain boundary resistance negligibly small. Here, the value of the low-frequency intersect was read as the total resistance, and the conductivity thereby determined are plotted in Fig. 3. It can be seen that regardless of the composition, the conductivities in moist atmosphere are obviously higher than those in the dry one. And the conductivities further increase with the partial pressure of water vapor

elevating from 0.05 atm to 0.30 atm (information on activation energy and pre-exponential factor is given in ESI). Such results indicate definitely the generation of proton conduction in moist atmosphere. **Fig. 4** compares the total conductivity at 600 and 700 °C in wet atmosphere. It is clear that $La_2(Nb_{0.3}Y_{0.7})_2O_{7-\delta}$ shows the highest conductivity, which is close to 1 $mScm^{-1}$ in the atmosphere with high moisture ( $p_{H_2O} = 0.30$ atm ) at 700 °C.

EMF measurements were performed to evaluate transport numbers of different charge carriers at 600 and 700 °C [32,33] (see Fig. S6 for measured EMF values). From Fig. 5, one can see that the apparent transport numbers of protons and oxide ions are dependent on composition, temperature and also atmosphere. Among the materials studied in this work, $La_2(Nb_{0.3}Y_{0.7})_2O_{7-\delta}$ shows the highest apparent transport numbers of ionic conduction ($t_{H^+} + t_{O^{2-}}$) and proton conduction ($t_{H^+}$), which are about 0.88 and 0.65 at 600 °C, and 0.83 and 0.34 at 700 °C, respectively, in wet $H_2$. It has to be noted that the effect of electrode polarization [32, 34] was not taken into consideration for compensation, so the actual transport numbers should be a little higher than the apparent ones. However, it can be said that $La_2(Nb_{1-x}Y_x)_2O_{7-\delta}$ ($x$ = 0.6, 0.65, 0.7) is not pure ionic conductors neither in wet oxygen nor in hydrogen atmosphere, but the transport properties can possibly be tuned by adopting proper doping strategy in future.

As aforementioned, $La_2(Nb_{1-x}Y_x)_2O_{7-\delta}$ is predicted to be chemically stable in $CO_2$, since there is no stable carbonates containing relevant elements of La, Nb or Y. To verify such prediction, the $La_2(Nb_{0.3}Y_{0.7})_2O_{7-\delta}$ sample after sintering was crashed into powder, and taken for example to expose

to the Ar atmosphere containing 10 vol% $CO_2$ and 5 vol% $H_2O$ at 500 -700 $^oC$ for 100 h. As expected, no second phase was detected (Fig. S7), indicating its quite excellent chemical stability.

In conclusion, a new ionic conductor of fluorite structure-based compound of $La_2(Nb_{1-x}Y_x)_2O_{7-\delta}$ ($x$ = 0.6, 0.65, 0.7) was discovered and reported to show proton conduction and superior chemical stability against $CO_2$ and $H_2O$. Among a couple of samples studied in this work, $La_2(Nb_{0.3}Y_{0.7})_2O_{7-\delta}$ shows the highest electrical conductivity and transport number of ionic conduction. As shown in Fig. 6, its conductivity is comparable with or even higher than some of the state-of-the-art proton conductors, including Ca-doped $LaNbO_4$ [12], $La_{6.63}W_{1.17}O_{13.43}$ [37], Sr-doped $LaP_3O_9$ [20]. However, $La_2(Nb_{0.3}Y_{0.7})_2O_{7-\delta}$ is not a pure proton conductor, and its conductivity is not sufficiently high. Further work with the aim to improve the transport properties is anticipated.

**Conflicts of interest**

There are no conflicts to declare.

## Notes and References

1 B.C.H. Steele, A. Heinzel, *Science*, 2001, **414**, 345.

2 S. Litster, G. McLean, *J. Power Sources*, 2004, **130**, 61.

3 R.M. Ormerod, *Chem. Soc. Rev.*, 2003, **32**, 17.

4 A.J. Jacobson, *Chem. Mater.*, 2010, **22**, 660.

5 W.G. Coors, *J. Power Sources*, 2003, **118**, 150.

6 H. Iwahara, T. Shimura, H. Matsumoto, *Electrochemistry*, 2000, **3**, 154.

7 K.D. Kreuer, *Annu., Rev. Mater. Res.*, 2003, **33**, 333.

8 E. Fabbri, D. Pergolesi, A. D'Epifanio, E. Di Bartolomeo, G. Balestrino, S. Licoccia, E. Traversa, *Energy. Environ. Sci.* 2008, **1**, 355.

9 Y. Yamazaki, R. Hernandez-Sanchez and S.M. Haile, *Chem. Mater.*, 2009, **21**, 2755.

10 D. Han, K. Shinoda, S. Sato, M. Majima and T. Uda, *J. Mater. Chem. A.*, 2015, 3, 1243.

11 D. Han, N. Hatada, T. Uda, *J. Electrochem. Soc.*, 2016, **163**, F470.

12 R. Haugsrud, T. Norby, *Nat. Mater.*, 2006, **5**, 193.

13 H. Matsumoto, Y. Kawasaki, N. Ito, M. Enoki, T. Ishihara, *Electrochem. Solid-State Lett.*, 2007, **10**, B77.

14 E. Fabbri, A. D'Epifanio, E. Di Bartolomeo, S. Licoccia, E. Traversa, *Solid State Ionics*, 2008, **179**, 558.

15 N. Yan, Y. Zeng, B. Shalchi, W. Wang, T. Gao, G. Rothenberg, J. Luo, *J. Electrochem. Soc.*, 2015,

**162**, F1408.

16 R. Sažinas, C. Bernuy-López, M. Einarsrud, T. Grande, *J. Am. Ceram. Soc.*, 2016, **99**, 3685.

17 T. Shimura, Y. Tokiwa, H. Iwahara, *Solid State Ionics*, 2002, **154-155**, 653.

18 A. Magrasó, M. Fontaine, R. Bredesen, R. Haugsrud, T. Norby, *Solid State Ionics*, 2014, **262**, 382.

19 T. Norby, A. Magrasó, *J. Power Sources*, 2015, **282**, 28.

20 K. Amezawa, Y. Uchimoto, Y. Tomii, *Solid State Ionics*, 2006, **177**, 2407.

21 N. Hatada, K. Toyoura, T. Onishi, Y. Adachi, T. Uda, *J. Phys. Chem. C*, 2014, **118**, 29629.

22 Y. Adachi, N. Hatada, A. Kuramitsu, T. Uda, *J. Electrochem. Soc.*, 2015, **162**, F596.

23 Y. Adachi, N. Hatada, T. Uda, *Int. J. Hydrogen Energy*, 2016, **41**, 21450.

24 A. Magrasó, C. Frontera, D. Marrero-López, P. Núnez, *Dalton Trans.*, 2009, 10273.

25 A. Magrasó, J.M. Polfus, C. Frontera, J. Canales-Vázquez, L. Kalland, C.H. Hervoches, S. Erdal, R. Hancke, M.S. Islam, T. Norby, R. Haugsrud, *J. Mater. Chem.*, 2012, **22**, 1762.

26 G. Kojo, Y. Shono, H. Ushiyama, Y. Oshima, J. Otomo, *J. Solid State Chem.*, 2017, **248**, 1.

27 L. Cai, A.L. Arias, J.C. Nino, *J. Mater. Chem.*, 2010, **21**, 3611.

28 V. Besikiotis, S. Ricote, M.H. Jensen, T. Norby, R. Haugsrud, *Solid State Ionics*, 2012, **229**, 26.

29 C. Hiraiwa, D. Han, A. Kuramitsu, A. Kuwabara, H. Takeuchi, M. Majima and T. Uda, *J. Am. Ceram. Soc.*, 2013, **96**, 879.

30 D. Han, M. Majima, T. Uda, *J. Solid State Chem.*, 2013, **205**, 122.

31 D. Han, K. Shinoda, T. Uda, *J. Am. Ceram. Soc.*, 2014, **97**, 643.

32 D. Han, Y. Noda, T. Onishi, N. Hatada, M. Majima, T. Uda, *Int. J. Hydrogen Energy*, 2016, **41**, 14897.

33 K. Shitara, T. Moriasa, A. Sumitani, A. Seko, H. Hayashi, Y. Koyama, R. Huang, D. Han, H. Moriwake, I. Tanaka, *Chem. Mater.*, 2017, **29**, 3763.

34 V.V. Kharton, F.M.B. Marques, *Solid State Ionics*, 2001; **140**, 381.

35 D. Han, N. Hatada, T. Uda, *J. Am. Ceram. Soc*., 2016, **99**, 3745.

36 T. Hibino, K. Mizutani, T. Yajima, H. Iwahara, *Solid State Ionics*, 1992, **58**, 85.

37 A. Magrasó, C. Frontera, D. Marrero-López, Pedro Núnez, *Dalton Trans*, 2009, 10273.

38 D. Han, K. Kojima, M. Majima and T. Uda, *J. Electrochem. Soc.*, 2014, **161**, F977.

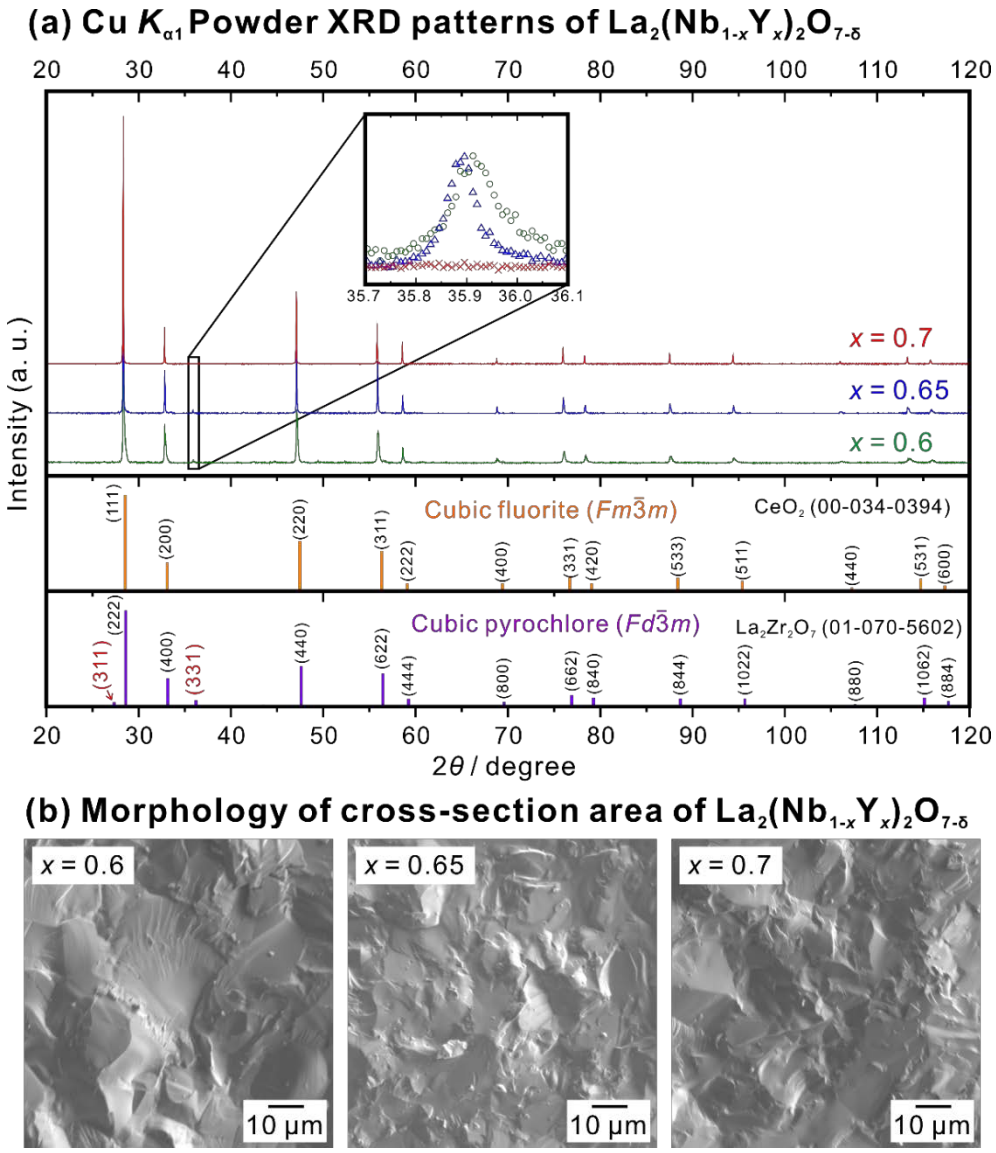


**Fig. 1** (a) Powder XRD patterns of as-sintered $La_2(Nb_{1-x}Y_x)_2O_{7-\delta}$ ($x$ = 0.6, 0.65, 0.7) collected with a monochromatic Cu $K\alpha_1$ X-ray source in ambient environment. References of $CeO_2$ (JCPDS # 00-034-0394) and $La_2Zr_2O_7$ (JCPDS # 01-070-5602) are plotted to show the difference between the cubic fluorite and cubic pyrochlore structures; that is, diffraction peaks of (331) and (311) raise in the XRD patterns of the cubic pyrochlore structures. (b) Second electron (EPMA-SE) images of the fractured cross-section of as-sintered $La_2(Nb_{1-x}Y_x)_2O_{7-\delta}$ ($x$ = 0.6, 0.65, 0.7) samples. All the samples were sintered at 1600 $^{o}$C in pure oxygen for 24 h.

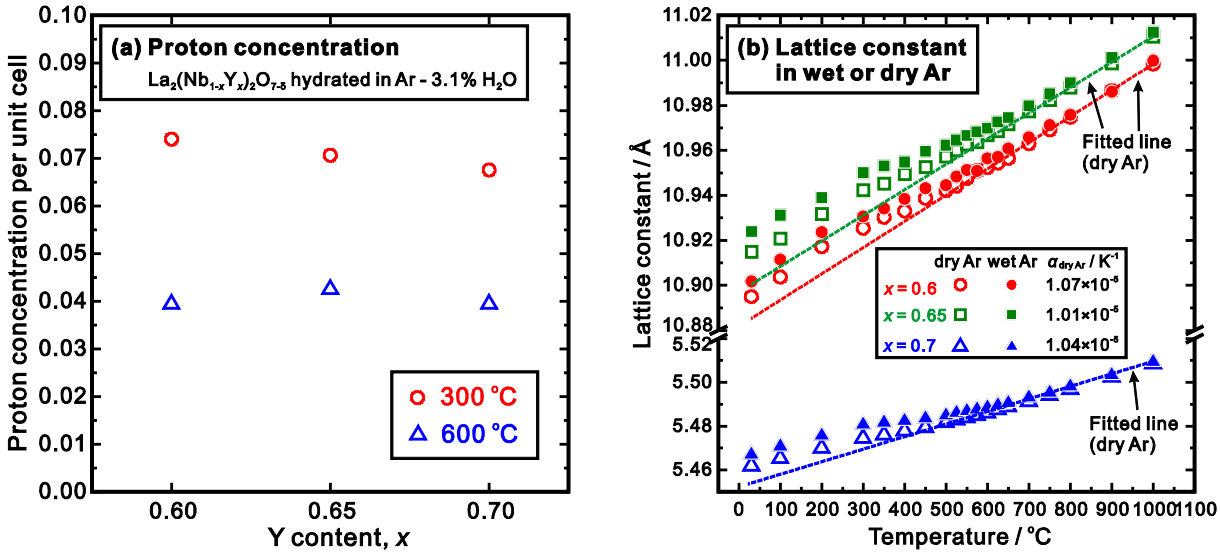


Fig. 2 (a) Proton concentration in $La_2(Nb_{1-x}Y_x)_2O_{7-\delta}$ ($x$ = 0.6, 0.65, 0.7) determined by measuring the water content in the samples hydrated in Ar – 3.1% $H_2O$ at 300 and 600 °C with the Karl-Fischer titration method. (b) Lattice constants of $La_2(Nb_{1-x}Y_x)_2O_{7-\delta}$ ($x$ = 0.6, 0.65, 0.7) in dry and wet Ar ($p_{H_2O} = 0.031$ atm) determined by simulating the powder HT-XRD patterns collected between 30 – 1000 °C with cubic pyrochlore ($Fd\bar{3}m$) and fluorite ($Fm\bar{3}m$) models for $La_2(Nb_{1-x}Y_x)_2O_{7-\delta}$ ($x$ = 0.6, 0.65) and $La_2(Nb_{0.3}Y_{0.7})_2O_{7-\delta}$, respectively. The thermal expansion coefficient ($\alpha_{dry\ Ar}$) were determined by linear fitting the lattice constants in dry Ar between 700 – 1000 °C (dashed lines).

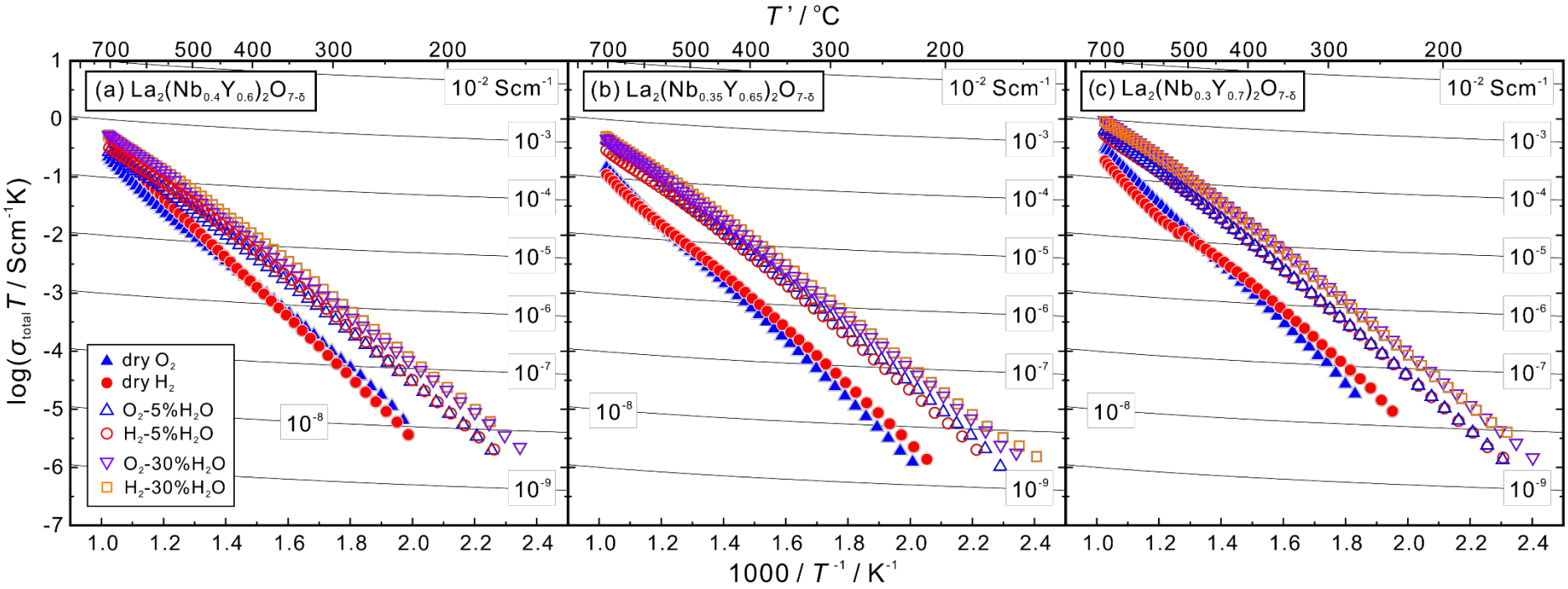


**Fig. 3** Arrhenius plots of total conductivities of $La_2(Nb_{1-x}Y_x)_2O_{7-\delta}$ ($x$ = 0.6, 0.65, 0.7) in dry or wet $O_2$ or $H_2$. The partial pressure of water vapor in the wet atmosphere was 0.05 or 0.30 atm by bubbling the gas through deionized water kept at 30 or 70 °C, respectively.

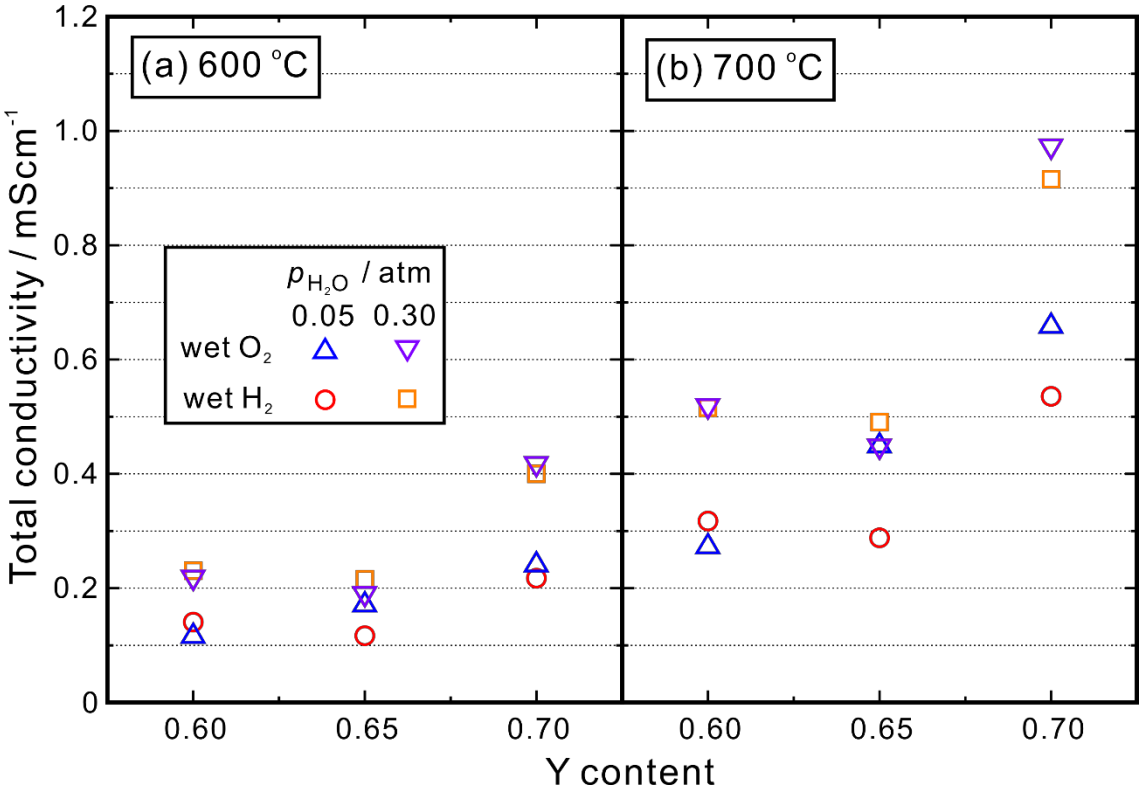


**Fig. 4** Total conductivity of $La_2(Nb_{1-x}Y_x)_2O_{7-\delta}$ ($x$ = 0.6, 0.65, 0.7) at (a) 600, and (b) 700 °C in wet $O_2$ or $H_2$. The partial pressure of water vapor in the wet atmosphere was 0.05 or 0.30 atm by bubbling the gas through deionized water kept at 30 or 70 °C, respectively.

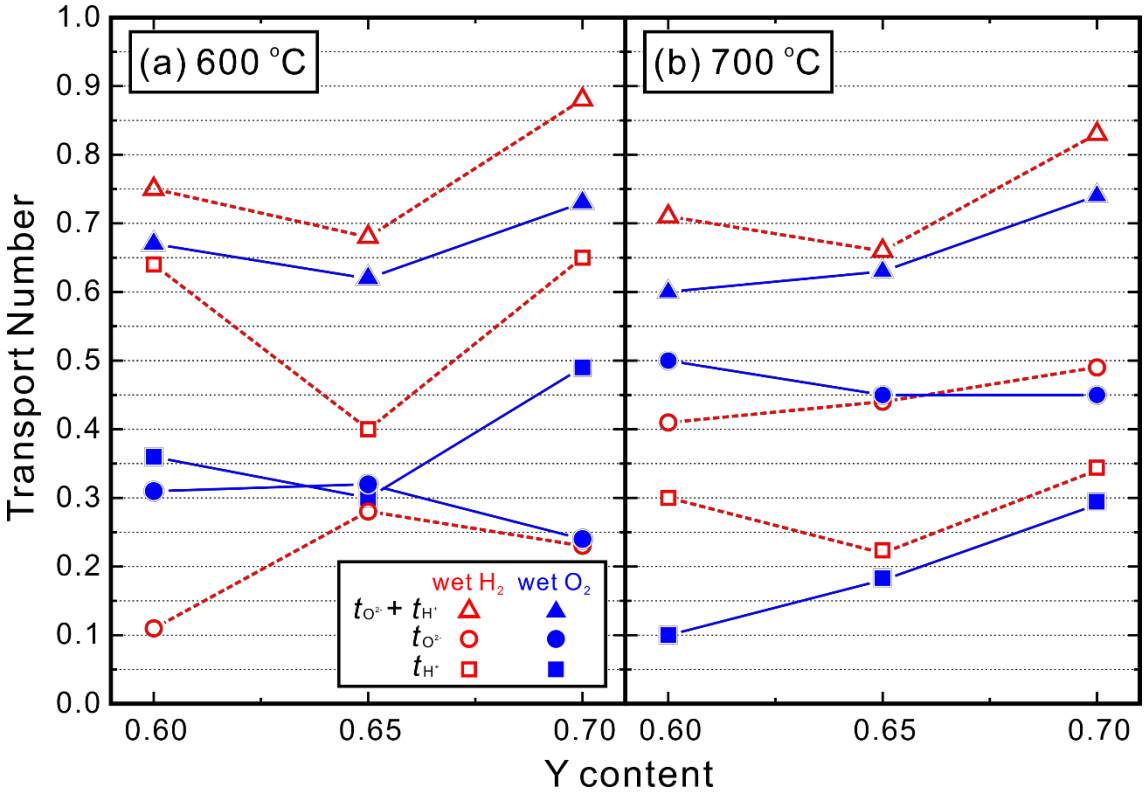


**Fig. 5** Apparent transport numbers of proton and ionic conduction in $La_2(Nb_{1-x}Y_x)_2O_{7-\delta}$ ($x$ = 0.6, 0.65, 0.7) at (a) 600, and (b) 700 °C. The transport numbers were determined by measuring the electromotive force of hydrogen concentration cells, oxygen concentration cells, and water vapor concentration cells. The effect of electrode polarization [32, 34] was not taken into consideration.

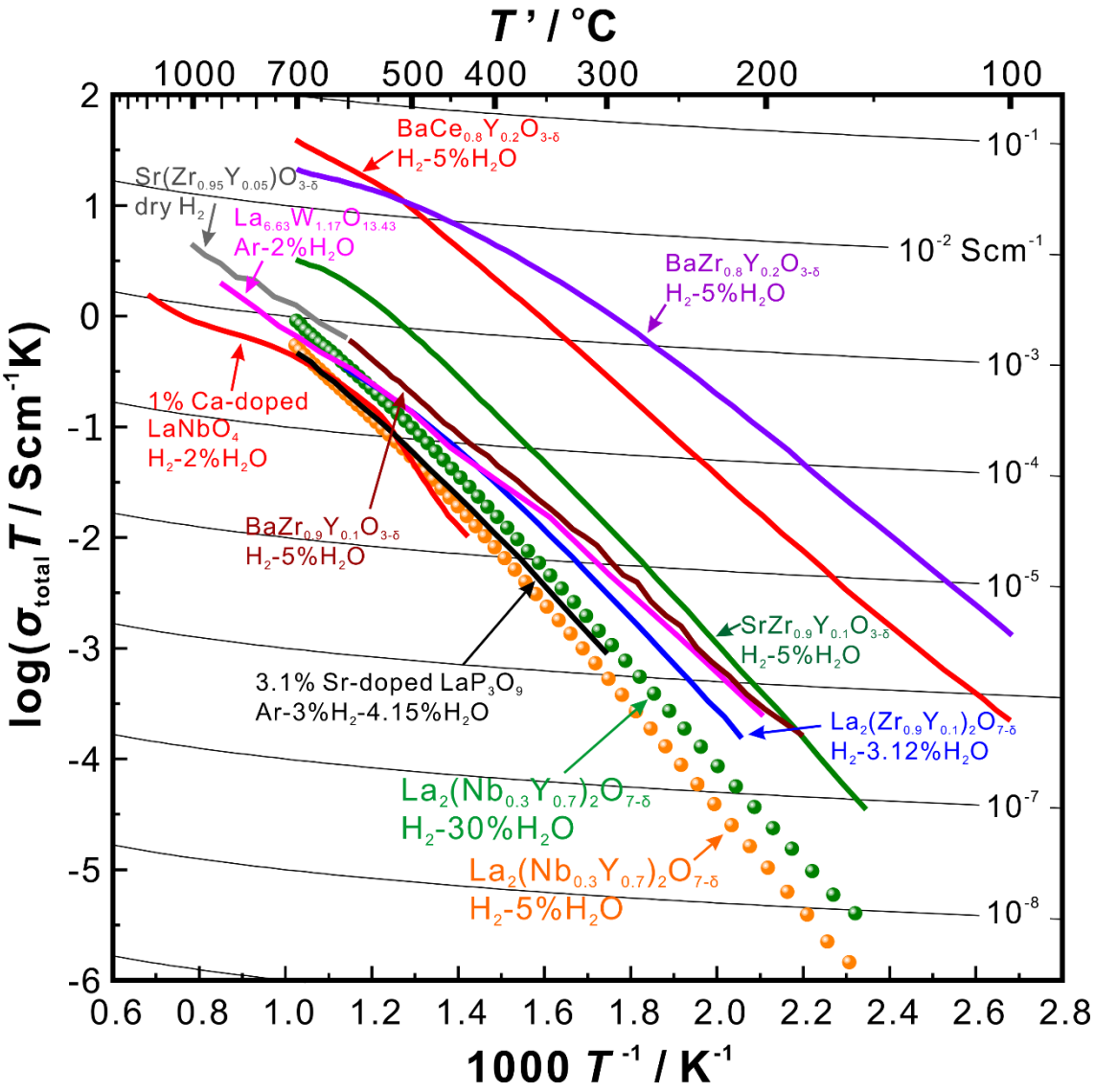


**Fig. 6** Total conductivities of $La_2(Nb_{0.3}Y_{0.7})_2O_{7-\delta}$ in wet $H_2$ ( $p_{H_2O}$ = 0.05 or 0.3 atm) in comparison with some representative state-of-the-art polycrystalline proton conductors, including $BaZr_{0.9}Y_{0.1}O_{3-\delta}$ [35], $SrZr_{0.95}Y_{0.05}O_{3-\delta}$ [36], $La_{6.63}W_{1.17}O_{13.43}$ [37], $La_2(Zr_{0.9}Y_{0.1})_2O_{7-\delta}$ [38], Ca-doped $LaNbO_4$ [12], Sr-doped $LaP_3O_9$ [20]. Conductivities of $BaZr_{0.8}Y_{0.2}O_{3-\delta}$, $BaCe_{0.8}Y_{0.2}O_{3-\delta}$ and $SrZr_{0.9}Y_{0.1}O_{3-\delta}$ were measured by the authors of this work, and are also plotted for comparison.